

# UC Santa Barbara

## UC Santa Barbara Previously Published Works

### Title

Highly efficient bacterial removal and disinfection by magnetic barium phosphate nanoflakes with embedded iron oxide nanoparticles

### Permalink

<https://escholarship.org/uc/item/6vz135b0>

### Journal

Environmental Science Nano, 5(6)

### ISSN

2051-8153

### Authors

Song, Junyi  
Zhang, Fan  
Huang, Yuxiong  
[et al.](#)

### Publication Date

2018

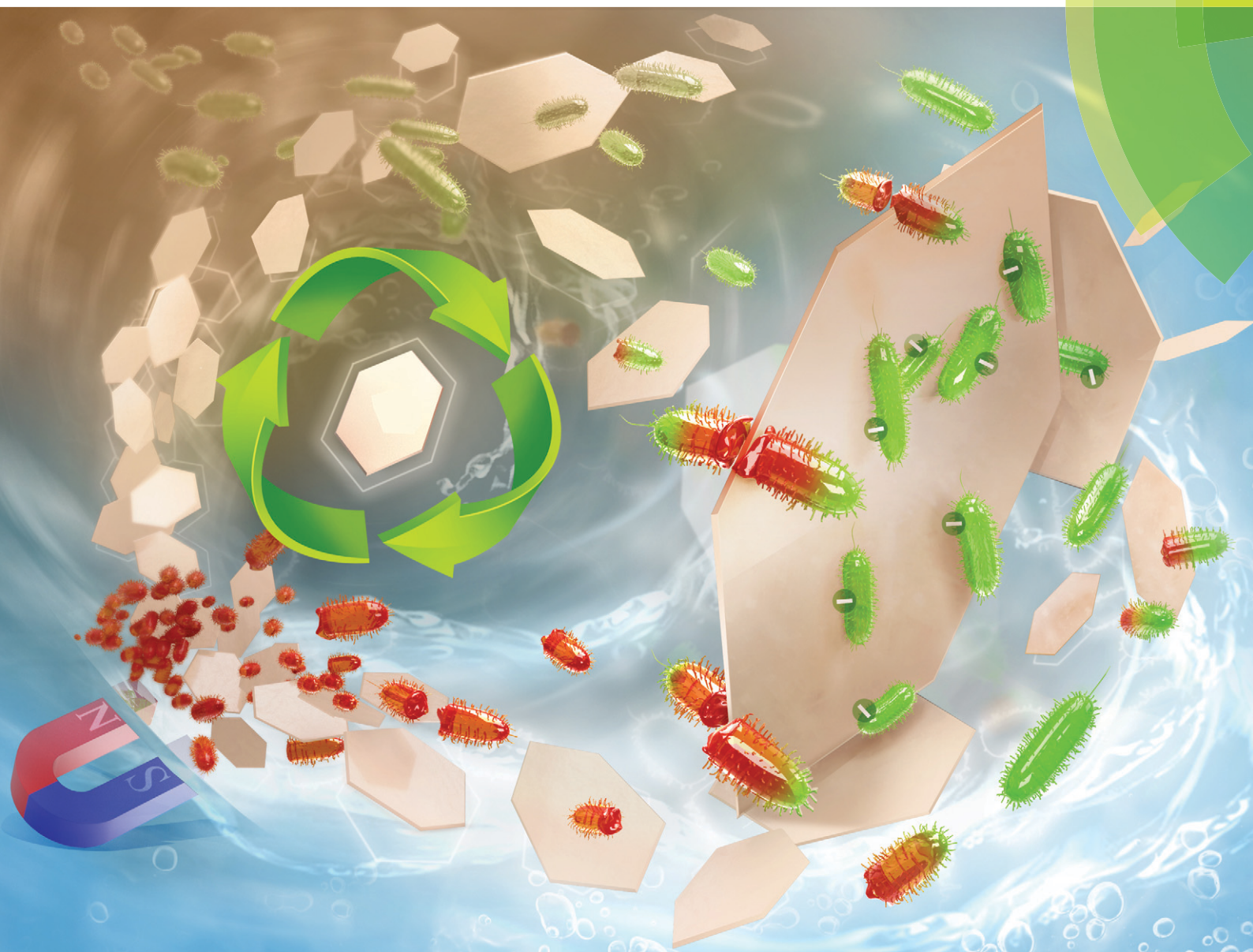
### DOI

10.1039/c8en00403j

Peer reviewed

# Environmental Science Nano

rsc.li/es-nano



ISSN 2051-8153



**PAPER**

Fan Zhang *et al.*

Highly efficient bacterial removal and disinfection by magnetic barium phosphate nanoflakes with embedded iron oxide nanoparticles



Cite this: *Environ. Sci.: Nano*, 2018, 5, 1341

## Highly efficient bacterial removal and disinfection by magnetic barium phosphate nanoflakes with embedded iron oxide nanoparticles†

Junyi Song,<sup>‡,ab</sup> Fan Zhang,<sup>‡,\*cd</sup> Yuxiong Huang,<sup>id</sup><sup>d</sup> Arturo A. Keller,<sup>d</sup> Xiaoxiu Tang,<sup>c</sup> Wanning Zhang,<sup>e</sup> Weibin Jia<sup>f</sup> and Jerome Santos<sup>b</sup>

Magnetic barium phosphate nanoflakes with embedded iron oxide nanoparticles,  $\text{Fe}_3\text{O}_4@\text{Ba}_3(\text{PO}_4)_2$  (denoted FBP), were prepared through a facile and inexpensive two-step process. FBP was used to purify water heavily contaminated with *E. coli* (initial concentration of  $5 \times 10^8$  CFU  $\text{mL}^{-1}$ ). FBP exhibited high removal efficiency (97%) within 30 min at 25 °C and pH 6. We investigated the effects of factors such as pH, ionic strength, co-existing anions, temperature, contact time, material dosage, and initial concentration of bacterial suspension, and developed optimized treatment conditions. The negligible effect of solution ionic strength on bacterial removal efficiency of FBP indicates its potential for microbial control even in high salinity water. Importantly, FBP can maintain a high bacterial removal efficiency of 87% after being reused for five cycles. FBP's magnetic properties allow an easy recovery from water. Several types of forces and mechanisms are thought to be involved in the bacterial removal process by FBP: electrostatic interactions, adhesion to FBP's planar surface, flocculation by polyvalent cations on FBP's surface, oxidation sterilization from  $\text{Fe}_3\text{O}_4$  in FBP, irreversible cell structural damage by FBP's edges and corners, and magnetic aggregation under a magnetic field. Thus, FBP is a promising material for effectively treating water with high microbial contamination.

Received 12th April 2018,  
Accepted 27th April 2018

DOI: 10.1039/c8en00403j

rs.c.li/es-nano

## 1. Introduction

Microbial contamination of drinking water supplies is a major emerging environmental issue around the world, and even low doses of pathogenic bacteria can pose severe threats

to public health, with potentially widespread impacts.<sup>1,2</sup> As an indicator of fecal contamination, *Escherichia coli* (*E. coli*) is commonly used to evaluate and monitor water quality.<sup>3</sup> Hence, it is common to evaluate the effectiveness of disinfection using the removal efficiency of *E. coli*. There is a need to

### Environmental significance

Contamination of drinking water with bacteria is a persistent public health problem around the world. We developed a novel magnetic barium phosphate nanoflake material (FBP) for efficient bacterial removal and disinfection of drinking water. FBP exhibits a much higher removal efficiency than comparable materials (nano and conventional). Importantly, it has potential for microbial control even under high salinity conditions (*e.g.* treated effluent). FBP can maintain a high bacterial removal efficiency after being reused for five cycles. Several types of forces and mechanisms were also discussed in detail. This work represents a key advance towards the facile synthesis and viable application of magnetic nanocomposites in treating water with high microbial contamination.

<sup>a</sup> College of Science, National University of Defense Technology, Changsha 410073, China

<sup>b</sup> Institute for Collaborative Biotechnologies, University of California, Santa Barbara, CA 93106, USA

<sup>c</sup> College of Sciences, Nanjing Agricultural University, Nanjing 210095, PR China. E-mail: zhangfan0128@njau.edu.cn; Fax: +86 25 84396098; Tel: +86 25 84396098

<sup>d</sup> Bren School of Environmental Science and Management, University of California, Santa Barbara, CA 93106, USA

<sup>e</sup> School of Chemistry and Chemical Engineering, Shanghai Jiao Tong University, Shanghai 200240, PR China

<sup>f</sup> College of Life Sciences, Nanjing Agricultural University, Nanjing 210095, PR China

† Electronic supplementary information (ESI) available: (1) Characterization experiment methods: optical microscopy, fluorescence-based cell live/dead test, SEM of *E. coli* with the materials, and dilution plate count method; (2) effects of temperature, interaction time, dosage, and initial *E. coli* concentration on bacterial removal; (3) comparisons of removal capacity for *E. coli* per mg material in this work with other recent reports; (4) zeta potentials of FBP and FNPs at different pH values, ionic strengths, co-existing anions, and cycles; (5) bacterial removal effect of rare barium phosphate nanoflakes; (6) dilution plating procedure results; (7) kinetics of the removal and disinfection process by FBP and FNPs; (8) confocal fluorescence images of *E. coli* cells treated in solutions containing metal ions released from FBP; (9) cell proliferation after treatment with FBP and FNPs; and (10) SEM images of *E. coli* with FBP and FNP treatment after magnetic separation. See DOI: 10.1039/c8en00403j

‡ These authors contributed equally.

develop novel biocides, since conventional biocides can become less and less efficient and effective due to the emergence of antibiotic-resistant strains.<sup>4</sup> Recently, a number of new materials or methods have been proposed to remove bacteria from water, for example, polyoxometalate supported ionic liquid phases,<sup>5</sup> single cell imprinting on Ag–Zn bimetallic nanoparticle modified graphene oxide sheets,<sup>6</sup> silver-modified zeolite,<sup>7</sup> cellulose nanofibers and activated carbon membranes,<sup>8</sup> pompon-like ZnO–PANI heterostructures,<sup>9</sup> electrocoagulation and electro-Fenton.<sup>10</sup> These materials showed removal and/or bactericidal properties. However, developing more sustainable materials for bacterial disinfection is still of great urgency and significance, especially with low cost and easy separation.

It has been proven that Fe<sub>3</sub>O<sub>4</sub> nanoparticles (denoted FNPs) generate reactive oxygen species (ROS) when interacting with bacteria, leading to protein oxidation and DNA damage, and finally resulting in cell death.<sup>11,12</sup> In addition, FNPs can be easily recovered from treated water in the post-treatment using a magnetic field.<sup>1,11,13</sup> However, if the FNPs do not possess strong bactericidal properties, the aggregates of FNPs that are not removed could then conceivably serve as anchoring points for further microbial colonization, which would bring up an undesired secondary contamination. Therefore, there have been an increasing number of studies to develop advanced functionalized magnetic nanocomposites for improving removal and disinfection of *E. coli* from contaminated water.<sup>13–16</sup> Magnetic graphene–carbon nanotube iron nanocomposites,<sup>13</sup> magnetic chitosan–graphene oxide composites,<sup>12</sup> anti-fimbrial modified magnetic reduced graphene oxide nanoheaters,<sup>17</sup> and Ag–CoFe<sub>2</sub>O<sub>4</sub>–GO nano-composites<sup>18</sup> have been reported to be effective adsorbents and antibacterial agents. However, these materials are generally used to purify *E. coli* contaminated water with an initial concentration range of 10<sup>2</sup>–10<sup>7</sup> colony forming units (CFU) per mL, and their removal capacities are limited to <10<sup>7</sup> CFU mg<sup>-1</sup>, which constrains their application range to moderately contaminated water. Furthermore, disinfection of *E. coli* from high-salinity wastewater using these magnetic nanomaterials is limited.

In a previous study we synthesized several types of magnetic phosphate nano-composites by a simple and inexpensive two-step method.<sup>19–22</sup> These materials exhibited high removal efficiency for several dyes (e.g. malachite green, Congo red, methyl blue) from water by hydrogen bonding, ionic interaction, and flocculation. Thus, there is a potential application for removing bacteria by magnetic phosphate nano-composites through similar interactions with different groups outside the cell membrane.

In this work, we applied a novel synthesis approach to prepare magnetic barium phosphate nanoflakes with embedded iron oxide nanoparticles, Fe<sub>3</sub>O<sub>4</sub>@Ba<sub>3</sub>(PO<sub>4</sub>)<sub>2</sub> (denoted FBP), which possess enhanced saturated magnetization (Ms) and surface area compared with our previous work.<sup>19</sup> The removal efficiency of *E. coli* by FBP nanoflakes was evaluated and compared with bare FNPs, under various environmental con-

ditions, including pH, temperature, reaction time, FBP dosage, and initial bacterial concentration, as well as the effects of ionic strength and competitive anions. In addition, the reusability of the FBP nanoflakes was examined through five consecutive bacterial removal cycles. The interactions between *E. coli* and magnetic materials were also investigated in detail by applying several characterization techniques.

## 2. Experimental

### 2.1. Materials and reagents

Ferric chloride (FeCl<sub>3</sub>·6H<sub>2</sub>O), sodium acetate (NaAc), polyethylene glycol 2000 (PEG 2000), ethylene glycol (EG), barium nitrate, cetyltrimethyl ammonium bromide (CTAB), sodium phosphate, sodium nitrate, sodium sulfate, sodium chloride, nitric acid, and sodium hydroxide were all purchased from Shanghai Sinopharm Chemical Reagent Co., Ltd. (China). All chemicals and reagents were of analytical grade and used as-received without any further purification.

### 2.2. Magnetic barium phosphate synthesis

In the first step, bare black FNPs were prepared using a solvothermal method: 1.35 g FeCl<sub>3</sub>·6H<sub>2</sub>O, 1 g PEG 2000, and 3.6 g NaAc were mixed with 40 mL EG by ultrasonic dispersion for 30 min at 30 °C. The mixed solution was transferred into two 50 mL Teflon-lined bottles held in a stainless-steel autoclave, sealed, and maintained at 200 °C for 5 h. After the autoclave cooled to room temperature, the powder was washed with deionized (DI) water and then with ethanol five times each. Then, the samples were dried in a vacuum oven at 60 °C for 3 h. In the second step, an olive magnetic FBP powder was obtained with a similar process: first, 0.06 g FNPs, 0.01 g CTAB, and 7.5 mmol barium nitrate were ultrasonically dispersed in 40 mL of DI water for 15 min at 30 °C. 5 mmol sodium phosphate was dissolved in 10 mL of DI water and then added dropwise slowly to the FNPs/CTAB/Ba(NO<sub>3</sub>)<sub>2</sub> suspension. CTAB and sodium phosphate were used as a versatile soft template and precipitant, respectively. After mechanical stirring for 30 min, the mixed suspension was transferred into two 50 mL Teflon-lined bottles, sealed, heated, cooled, washed, and dried with the same procedure as for the FNPs. At the end of the synthesis, around 1.3 g FBP were obtained at a cost of about \$0.08 per g, which indicates the economic efficiency and practicality of this material.

### 2.3. Characterization

Scanning electron microscopy (SEM) studies were performed using an FEI XL40 Sirion FEG digital scanning microscope with an Oxford energy dispersive spectroscopy (EDS) analysis system. Transmission electron microscopy (TEM) images were obtained *via* an FEI Tecnai G2 Sphera 200 kV Cryo. X-ray diffraction (XRD) patterns were obtained on a Bruker (model AXS D8, Germany) Advanced XRD. The specific surface area was measured with a N<sub>2</sub> adsorption isotherm by using an ASAP 2020 M Micromeritics instrument at 100 °C

and *via* the Brunauer–Emmett–Teller (BET) method. The corresponding zeta potential (ZP) values of the materials were determined *via* a ZP analyzer (Malvern, Model Nano ZS, England). The magnetic performance of the materials was investigated using a physical property measurement system (PPMS, Model-9, Quantum Design, USA). The released concentrations of  $\text{Fe}^{3+}$  and  $\text{PO}_4^{3-}$  into the solution from the materials during the removal process were analyzed with an inductively coupled plasma-atomic emission spectrometer (ICP-AES, Optima 2100, PerkinElmer, USA) and an ion chromatograph (Thermo, model ICS-5000), respectively.

#### 2.4. Bacterial suspension preparation

*E. coli* was cultivated in 100 mL of Luria Broth (LB) growth medium, consisting of  $10 \text{ g L}^{-1}$  tryptone,  $5 \text{ g L}^{-1}$  bacto-yeast extract, and  $10 \text{ g L}^{-1}$  NaCl. The strain was shaken at 220 rpm and  $37^\circ\text{C}$  in a thermostatic incubator until the logarithmic growth late phase was reached. Cells were then separated from the growth medium by centrifugation (6000 rpm for 5 min at  $15^\circ\text{C}$ ). The bacterial pellets were washed three times with sterilized DI water to remove the residual growth me-

diium and were then re-suspended in sterilized DI water to obtain bacterial stock solutions with a cell density of approximately  $5 \times 10^8 \text{ CFU mL}^{-1}$ . The concentration of the bacterial suspension was established using the optical density at 600 nm ( $\text{OD}_{600}$ ) measured with a Shimadzu (Japan, model UV1700) ultraviolet spectrophotometer.

#### 2.5. *E. coli* removal

Generally, 0.1 g of either FBP or FNPs was added to 50 mL of *E. coli* suspension ( $5 \times 10^8 \text{ CFU mL}^{-1}$ ) at  $25^\circ\text{C}$  and pH 6.0 with mechanical stirring for 30 min to investigate the removal efficiency. The pH value was adjusted from 5 to 9 to study its effect on *E. coli* removal efficiency. To investigate the influence of temperature and dosage of the materials, the studies were done at different temperatures ( $10, 15, 20, 25, 30, 35, 40^\circ\text{C}$ ) and dosages (0.02 g, 0.05 g, 0.08 g, 0.10 g, 0.15 g). A kinetic study was conducted by changing the interaction time (2, 5, 10, 20, 30, 40, 50 min). The maximum removal capacity of the magnetic materials (FBP and FNPs) was evaluated *via* adjusting the initial concentration of *E. coli* ranging from  $2.5 \times 10^8$  to  $12.5 \times 10^8 \text{ CFU mL}^{-1}$ . A neodymium magnet

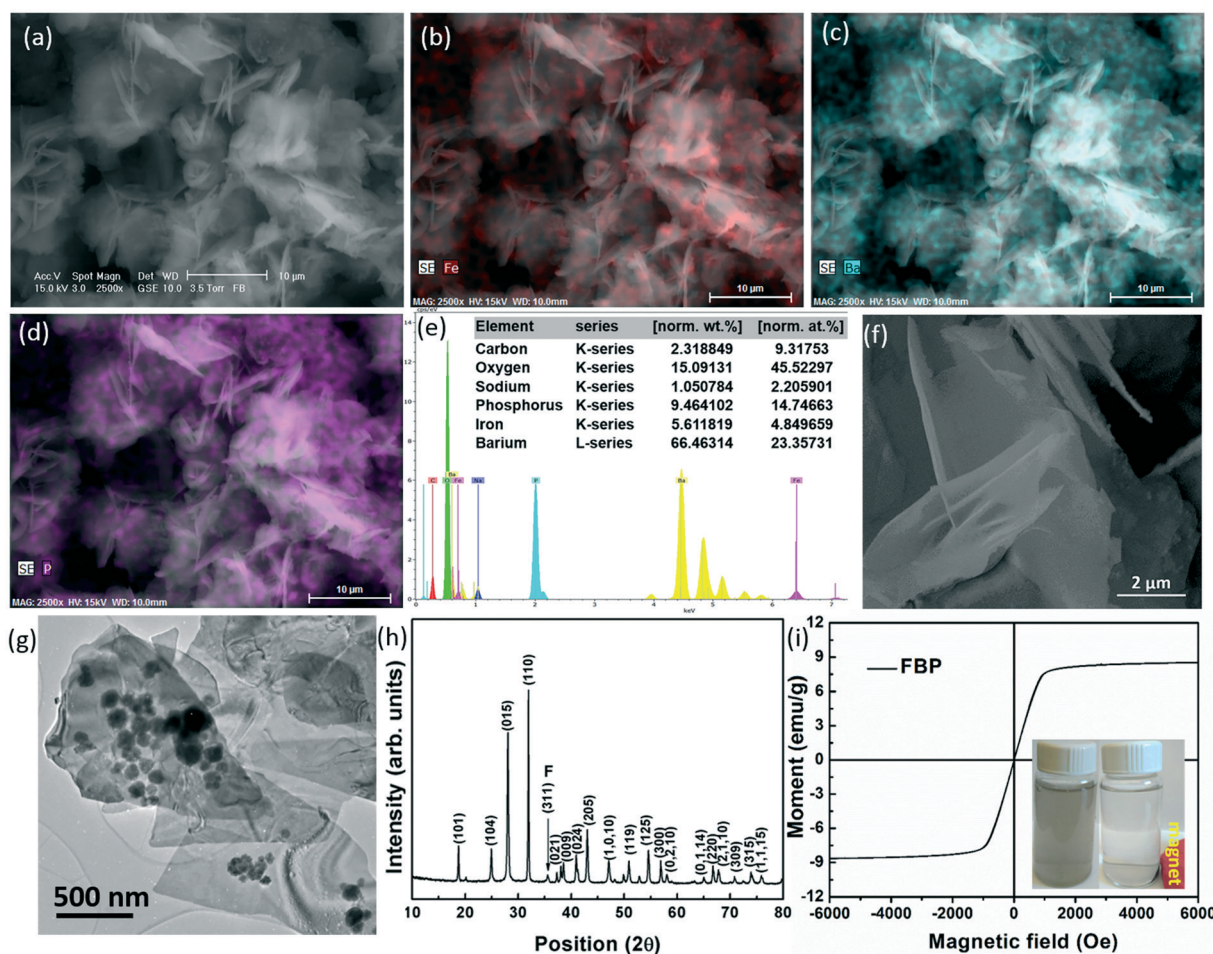


Fig. 1 (a) SEM image of FBP; corresponding element mapping of (b) Fe, (c) Ba, and (d) P in FBP; (e) EDS results, (f) SEM close-up image of FBP, (g) TEM image of FBP, (h) XRD pattern and (i) magnetic properties of FBP.

(diameter of 50 mm, thickness of 5 mm) was used to separate the bacteria-loaded material from the aqueous solution, and the residual concentration of *E. coli* was calculated via OD<sub>600</sub>. To evaluate the reusability of FBP, the bacteria-loaded FBP particles from the first cycle were directly added to the same bacterial suspension to start the next treatment under the same experimental conditions. This was repeated for 5 cycles. All experiments were repeated three times and the average and standard deviation were reported. The interactions between *E. coli* and the magnetic materials were analyzed using an optical microscope, SEM, confocal fluorescence images, and dilution plate counting. The related experimental methods are described in the ESI.†

### 3. Results and discussion

#### 3.1. Characterization of materials

As seen from the SEM images of FBP (Fig. 1a and f), FBP exhibits a flake-like structure with sharp edges and corners. The thickness is around 40 nm and the length is around 7 μm, which is larger than the length of an *E. coli* cell (700 nm–1.2 μm).<sup>18</sup> The plane and large flakes of FBP improve the adhesion of *E. coli* to its surface. EDS results (Fig. 1e) demonstrate the presence of Fe, with a content of 4.85% in the FBP nanoflakes. The element mapping results (Fig. 1b–d) confirm the uniform distribution of Fe, Ba, and P in the composites. From the EDS X-ray scan, which can go to a depth of up to 2 μm under the surface, Fe was uniformly distributed inside the nanoflakes rather than simply adhering physically to the surface or blending into the barium phosphate. This may reduce atmospheric air oxidation and acid corrosion of the embedded FNPs within FBP.<sup>18</sup> The morphology of the FBP nanoflakes was further examined using TEM. Fig. 1g shows a thin FBP nanoflake with sharp edges and corners, with embedded FNPs. Pure FNPs possess a spherical shape with an average size of ~100 nm (Fig. S1†). Hence, FNPs are much smaller than an *E. coli* cell, and they may attach to the *E. coli* cell surface.

On the basis of the XRD data (Fig. 1h), the main characteristic peaks are attributed to the diffraction of rhombohedral crystal planes of Ba<sub>3</sub>(PO<sub>4</sub>)<sub>2</sub> (JCPDS No. 25-0028).<sup>23</sup> The small peak marked at 35.8° confirmed the presence of Fe with a relatively lower concentration in the composites. The sharp peaks revealed the fine crystallinity of the FBP nanoflakes.<sup>23</sup> As shown in Fig. 1i, the magnetic saturation (*M*<sub>s</sub>) of FBP is around 8.7 emu g<sup>-1</sup>, which is higher than similar magnetic bactericides<sup>18</sup> and FBP from a previous study with larger iron oxide particles.<sup>19</sup> A strong magnetic response results in easier and faster post-treatment separation, as shown in the embedded picture in Fig. 1i. More than 94% of FBP can be separated from water with a small neodymium magnet within 1 min. The surface area of FBP is 48 m<sup>2</sup> g<sup>-1</sup>, which is three times higher than the surface area of barium phosphate blended iron oxide submicron particles (14.8 m<sup>2</sup> g<sup>-1</sup>) reported previously.<sup>19</sup> This can improve *E. coli* removal because FBP's larger surface area provides more exposed active sites for adhesion.

#### 3.2. Removal of *E. coli* using FBP and FNPs

A series of experiments were conducted to investigate the influence of different factors such as temperature, time interval, dosage, initial concentration, and pH on *E. coli* removal using FBP. There was no substantial temperature effect on *E. coli* removal efficiency from 10 °C to 40 °C (Fig. S2†). Improved removal efficiency was obtained when the FBP dosage was increased from 0.02 g to 0.10 g, while the increased initial concentration of *E. coli* led to decreased removal efficiency (Fig. S3 and S4†). On the basis of the optimized treatment conditions, the removal capacity of the FBP nanoflakes (2.43 × 10<sup>8</sup> CFU mg<sup>-1</sup>) is higher than those of many previous studies (Table S1†), demonstrating the high potential of FBP nanoflakes for treating water heavily contaminated with bacteria.

Fig. 2 shows the effect of pH on the removal of *E. coli* by FBP and FNPs. Bacterial cells possess a negative surface charge within a pH range of 5.0–9.0,<sup>1</sup> while FBP exhibits a positive ZP at pH < 7 and the isoelectric point of FNPs is slightly above 6 (Fig. S5†). Thus, the slightly decreased removal efficiency of FBP from 96% to 84% may be due to the change in the particle's surface charge (Fig. S5†), which implies that electrostatic interaction is the driving force in the removal process. A similar phenomenon was also reported in a previous study with amine-modified magnetic nanoparticles.<sup>1</sup> The negligible effect of pH on the removal efficiency of FNPs in the tested pH range implies that the electrostatic forces between FNPs and *E. coli* were weak.

The ionic strength of the suspension also influences the surface charge of bacteria and particles, and thus affects the electrostatic interaction between bacterial cells and particle surfaces.<sup>4</sup> As shown in Fig. 3, more than 95% of *E. coli* cells could be removed by FBP over the entire range of ionic strength tested (0–1000 mM NaCl), indicating that no significant effect was induced by changes in ionic strength. This can be explained by the positive surface charge of FBP over

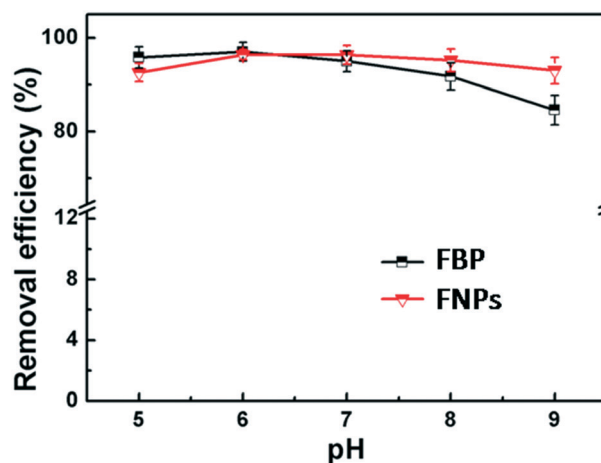


Fig. 2 Removal efficiency of *E. coli* (initial concentration,  $C_0 = 5 \times 10^8$  CFU mL<sup>-1</sup>, 25 °C, 30 min) using 2.0 mg mL<sup>-1</sup> FBP or FNPs at different pH values ranging from 5 to 9.

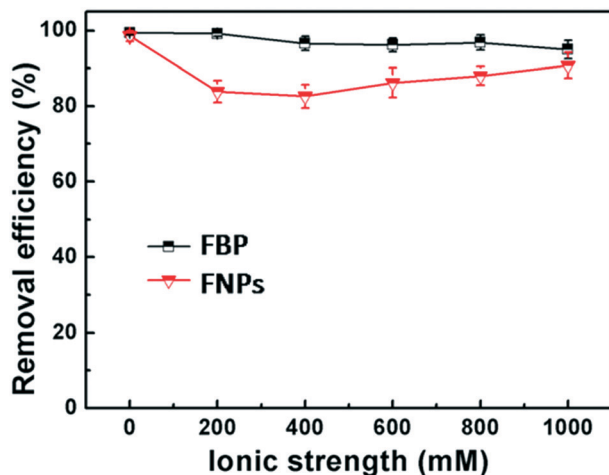


Fig. 3 Effect of ionic strength (0–1000 mM NaCl) on *E. coli* removal efficiency ( $C_0 = 5 \times 10^8$  CFU mL<sup>-1</sup>, 25 °C, pH 6, 30 min) with a dose of 2.0 mg mL<sup>-1</sup> FBP and FNPs.

the entire ionic strength range examined (Fig. S6†) which is beneficial to the attachment of negatively charged *E. coli* onto FBP's surface *via* electrostatic interaction. Therefore, FBP can be applied to separate bacteria from high-salinity water.

However, the increase in ionic strength from 0 to 400 mM led to the significant reduction of the removal efficiency of FNPs. This is due to the transition of the ZP of FNPs from positive to negative values as the ionic strength increases (Fig. S6†). The enhanced repulsion between *E. coli* and FNPs can result in a decrease in removal efficiency. The gradual increase in the removal efficiency of FNPs at an ionic strength higher than 600 mM (Fig. S6†) could be ascribed to the decrease in electrostatic repulsion between *E. coli* and FNPs. A similar phenomenon was also reported for interactions between biphasic calcium phosphate ceramic and protein.<sup>24</sup>

Anions, including sulfate, phosphate, and nitrate, are commonly present in surface water and groundwater.<sup>4</sup> These coexisting anions might adsorb onto the surface of the nano-materials and affect the bacterial attachment process.<sup>25</sup> The typical concentrations of sulfate, phosphate, and nitrate in

natural water are usually lower than 10 mM.<sup>26</sup> Therefore, the effects of these anions in a concentration range of 0–10 mM on the bacterial capture efficiency of FBP and FNPs were investigated in this work. As shown in Fig. 4, the presence of sulfate and nitrate did not have substantial effects on the removal efficiency of *E. coli* by FBP, while increasing the concentration of phosphate from 0 to 10 mM decreased FBP's *E. coli* removal ability from 98% to 67%. The ZP of bacteria was negative under all examined conditions regardless of the type of anion or concentration level.<sup>4</sup> Although the ZP of FBP was influenced by the presence of the anions at different concentrations (Fig. S7†), the ZP remained positive at almost all concentrations of sulfate or nitrate, which resulted in a consistent bacterial removal efficiency of FBP in the presence of these anions. Given its large negative charge, phosphate can be easily adsorbed onto the positively charged surface of FBP, leading to a decreased number of active sites on FBP's surface. Therefore, the bacterial removal efficiency of FBP decreased as the phosphate concentration increased. For FNPs, the increasing concentration of sulfate, phosphate, or nitrate resulted in decreased removal efficiency of *E. coli*, especially with the addition of nitrate. The adsorbed anions on the surface of FNPs may lead to a major shift in their surface ZP from positive to negative (Fig. S7†) and enhance the repulsive energy barriers for *E. coli* to attach onto the surface of FNPs. However, it should be noted that the typical concentrations of phosphate and nitrate in natural water are usually below 1 mM.<sup>25</sup> Thus, FBP and FNPs would effectively capture bacterial cells from natural water with the typical concentrations of the coexisting anions.<sup>25</sup> In the case of the co-existence of phosphate and nitrite at elevated concentrations, a high bacterial removal efficiency may still be obtained by increasing the material dosage (Fig. S3†).

### 3.3. Flocculation effect

In order to understand the interaction between *E. coli* and the magnetic materials, optical microscopy was employed. The images show that pure *E. coli* cells before treatment are dispersed homogeneously (Fig. 5a). After being treated with

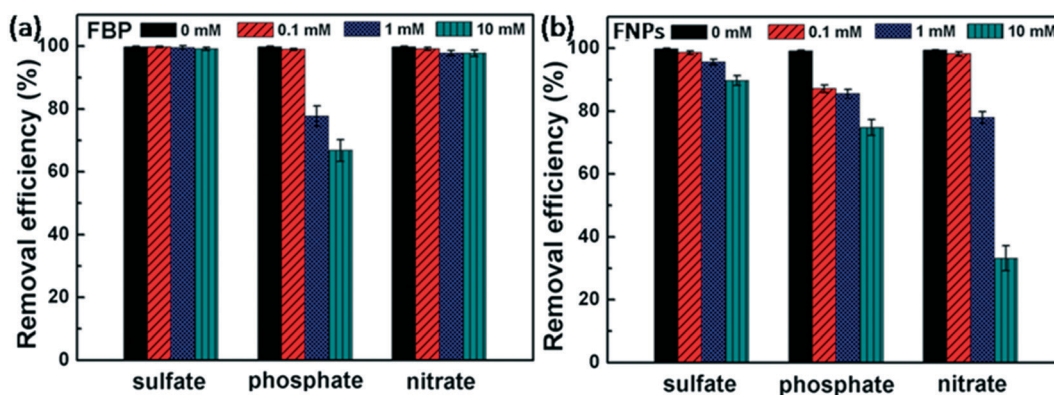


Fig. 4 Effect of anions on the removal efficiency of *E. coli* ( $C_0 = 5 \times 10^8$  CFU mL<sup>-1</sup>, 25 °C, pH 6, 30 min) with a dose of 2.0 mg mL<sup>-1</sup> (a) FBP and (b) FNPs.

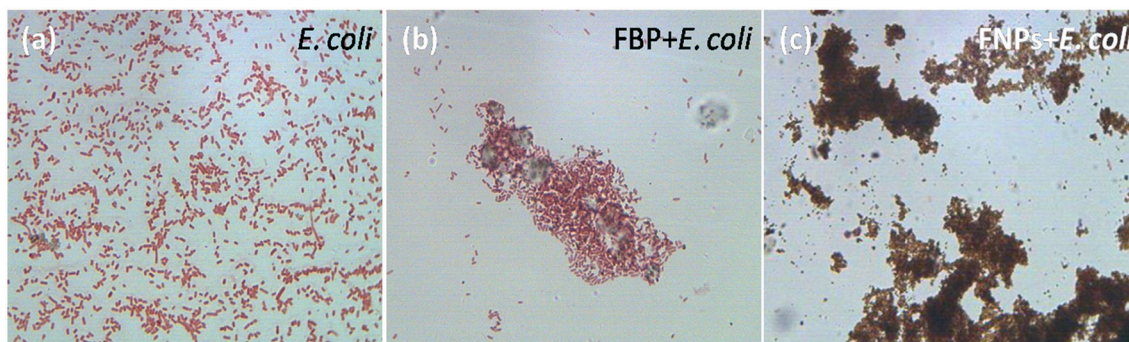


Fig. 5 Optical microscopy images of (a) pure *E. coli*, *E. coli* adhered to (b) FBP and (c) FNPs after treatment ( $C_0 = 5 \times 10^8$  CFU mL<sup>-1</sup>, 25 °C, pH 6, material dosage 2.0 mg mL<sup>-1</sup>, 30 min).

FBP (Fig. 5b) and FNPs (Fig. 5c), the bacterial cells aggregated substantially onto the magnetic materials. This was evidenced by the large agglomerates of bacteria (red) and the magnetic materials (black). The surface charge of bacteria is opposite to that of the magnetic materials at pH 6. Therefore, flocs of polyvalent cations on the surface of the magnetic material and the negative cell membrane form rapidly due to charge neutralization, which agrees with previous studies.<sup>4,27</sup> Importantly, a smaller area of the material and a larger area of bacteria can be observed in Fig. 5b compared with Fig. 5c, which implies that FBP is more effective in flocculating *E. coli* than the FNPs. Electrostatic interaction may aid substantially in the flocculation due to charge neutralization.<sup>27</sup> The polyvalent cations on FBP's surface can promote flocculation and accelerate the removal of bacteria.<sup>27,28</sup> This may be due to the fact that FBP nanoflakes possess more polyvalent cations and more positively charged surfaces than FNPs. It should be noted that pure Ba<sub>3</sub>(PO<sub>4</sub>)<sub>2</sub> nanoflakes showed a lower removal efficiency (61%) for *E. coli* (Fig. S8†) than FBP though they shared a similar shape and surface area.<sup>23</sup> Therefore, the flocculation effect from the iron in FBP (e.g. iron nanoparticles, iron ions, iron oxides, and hydrolysis products) contributes to *E. coli* removal.<sup>27,28</sup> Furthermore, PO<sub>4</sub><sup>3-</sup> groups associated with FBP can combine with H<sup>+</sup> to help release Fe<sup>3+</sup> and Fe<sup>2+</sup>; this can increase the flocculation effect of FBP as hydrolysis products (e.g. [Fe(OH)]<sup>2+</sup>, [Fe(OH)<sub>2</sub>]<sup>+</sup>, [Fe(OH)]<sup>+</sup>) can also produce agglomeration of microorganisms.<sup>27</sup>

### 3.4. Reuse of FBP and FNPs

The recovery and reuse of FBP and FNPs throughout five consecutive bacteria removal experiments are illustrated in Fig. 6. It can be observed that the *E. coli* removal efficiencies of both FBP and FNPs were more than 90% in the first cycle, and then decreased slowly after each cycle. This tendency can be explained by the fact that the materials were covered by more bacteria after additional cycles, which can result in decreased surface charge from positive to negative values (Fig. S9†) and fewer sites available for other bacterial attachment. However, FBP still removes around 87% of *E. coli* after five cy-

cles and FNPs remove 86% under the same conditions. Thus, the electrostatic interaction may be not the dominant mechanism for the high removal efficiency during the reuse.

The chemical stability of the magnetic materials and the retention of adsorbed bacteria are significant in the reuse process to avoid secondary pollution (from the release of components of FBP, FNPs or bacteria) in the treated water.<sup>18</sup> On the basis of ICP-AES and ion chromatography analysis, there was no significant release of Fe<sup>3+</sup> or PO<sub>4</sub><sup>3-</sup> into the solution from the magnetic materials during the five cycles, which demonstrates the chemical stability of FBP and FNPs in the removal process. After bacterial treatment, FBP and FNPs were rinsed with 50 mL of sterilized DI water three times to determine whether the captured bacteria on the surface of these materials could be released back into the environment, resulting in secondary pollution. On the basis of dilution plate count results (Fig. S10†), FBP that had been loaded with bacteria released less live *E. coli* (0.48%) into solution than FNPs (0.96%). This may be due to the stronger electrostatic binding and flocculation by FBP or the better disinfection effect of FBP. Furthermore, after being rinsed ultrasonically for 5 min, FBP acquired a positive surface charge

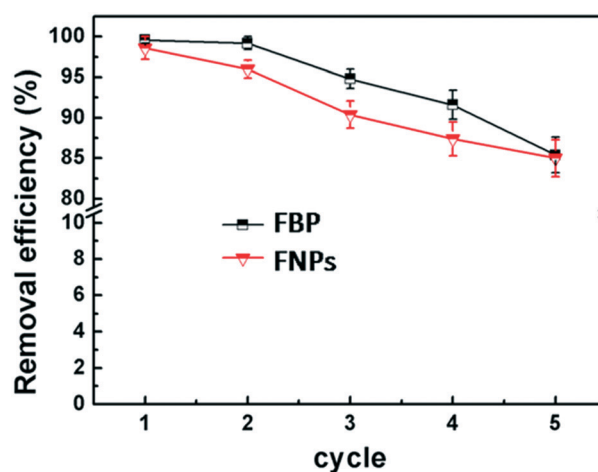


Fig. 6 Removal efficiency of *E. coli* at different cycles ( $C_0 = 5 \times 10^8$  CFU mL<sup>-1</sup>, 25 °C, pH 6, 30 min) with an initial dosage of 2.0 mg mL<sup>-1</sup> FBP and FNPs.

again, which implies that the captured cells were washed off and the materials could be reused.

### 3.5. Disinfection effect

In order to confirm whether the cells were affected by the magnetic materials in a reversible manner or not, fluorescence-based cell tests of live and dead bacterial cells were conducted (Fig. 7). The strong green fluorescence intensity region (Fig. 7a and d) represents the proportion of live and dead bacteria, and the heavy red fluorescence intensity region (Fig. 7b and e) indicates the dead fraction.<sup>18</sup> It can be clearly observed from Fig. 7b that most of the bacteria adhered to FBP's surface are dead, indicating irreversibly damaged cell membranes or mass cell death upon exposure to FBP.<sup>3</sup> However, most of the bacterial cells were still alive after being treated with FNPs (Fig. 7d and e).

The removal kinetics are shown in Fig. S11 and S12.† The maximum removal was achieved after 30 min, with no substantial improvement with longer times. The kinetic behavior of the disinfection process was determined by considering the disinfection at different time intervals; the confocal fluorescence images were used to evaluate the ratio of live and dead bacterial cells treated with FBP and FNPs. As shown in Fig. S13,† around 30%, 70%, and 90% of bacteria were inactivated after treatment with FBP under shaking for 5 min, 10 min, and 30 min, respectively. However, FNPs showed a lower disinfection ratio (less than 40%) after 30

min (Fig. S14†) under shaking compared with FBP under shaking (Fig. S13†).

FBP under mechanical stirring (Fig. 7) or shaking (Fig. S13g–i†) generated a similar disinfection effect, implying that the stirring paddle itself was not likely the cause of cell death. Furthermore, without any mechanical mixing, FBP resulted in much lower disinfection (less than 20%) (Fig. S15†) than FBP under mechanical stirring (Fig. 7) or shaking (Fig. S13†). This implies that the mechanical mixing process can improve FBP's physical bactericidal action because it allows more bacteria to be in contact with the sharp FBP nano-flake edges. The pure cations ( $\text{Fe}^{2+}$ ,  $\text{Fe}^{3+}$ , or  $\text{Ba}^{2+}$ ) showed no noticeable toxicity to *E. coli* (Fig. S16†). Once the cell membrane is broken by FBP, ROS or some cations in solution can react with protein, DNA, or other matters inside the cell, leading to cell death.

Dilution plate count assay was conducted to measure cell proliferation after treatment with FBP and FNPs (Fig. S17†). Cell proliferation was weakest for the treatment using FBP under stirring, which is consistent with confocal fluorescence microscopy results. To further investigate the underlying mechanism and inspect the bacterial morphological change, *E. coli* cells adhered to FBP and FNPs were visualized using SEM. Compared with pure *E. coli* (Fig. S18a†), most of the bacterial cells fused onto the FBP surface with an irregular shape (Fig. S18b†) which seemed to exhibit a plasmolysis phenomenon.<sup>18,28</sup> Only a small number of *E. coli* cells were found fixed on the FBP plane (Fig. S18c and d†). But some of

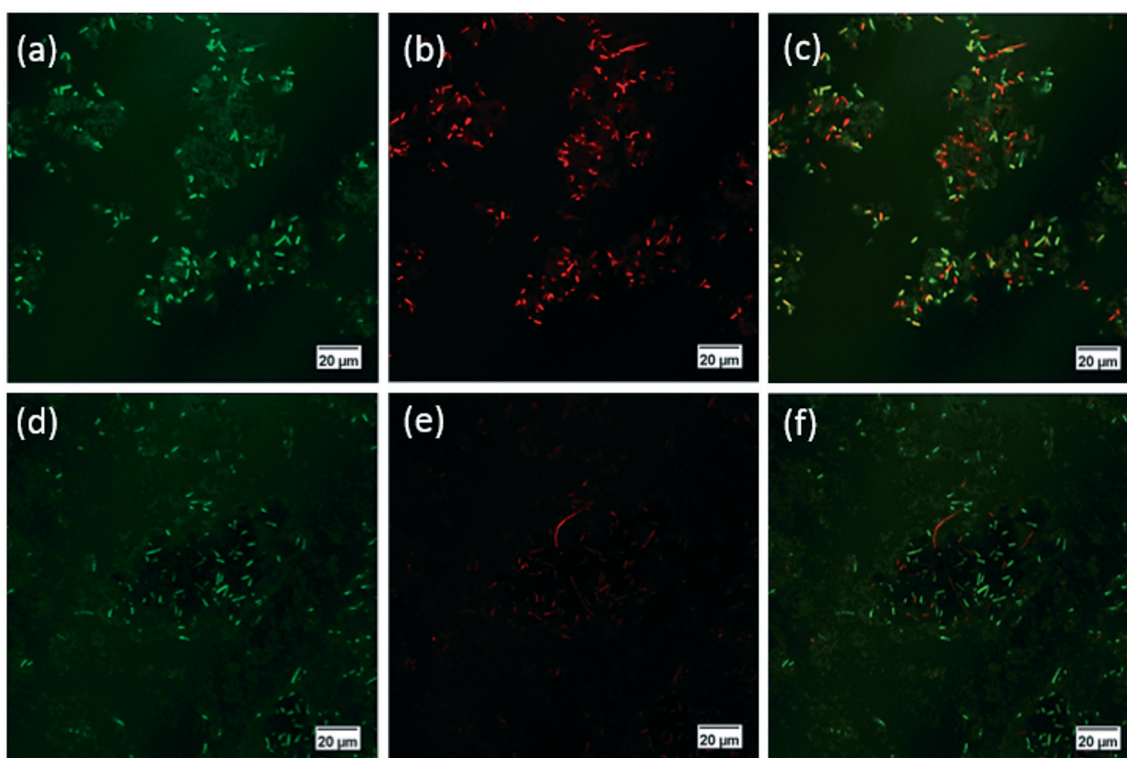


Fig. 7 Confocal fluorescence images of live and dead bacterial cells treated with FBP (a–c) and FNPs (d–f) under mechanical stirring and stained with SYTO9 (green) and PI (red). (c and f) Overlaid images of *E. coli* stained with SYTO9 (live and dead) and PI (dead).

the cell membranes were deformed from the normal rods to round shapes. Similar results were seen in other antibacterial materials, such as magnetic chitosan–graphene oxide composites and graphene-based antibacterial paper.<sup>12,29</sup> The leakage of intracellular constituents and change of morphology may be due to altered cell permeability resulting from the interaction between positively charged FBP and the negatively charged membrane of cells.<sup>30</sup> Moreover, iron oxide nanoparticles have been shown to generate ROS when interacting with bacteria, resulting in protein oxidation and cell death.<sup>31,32</sup> Additionally, *E. coli* cells were observed to be divided into two parts after being in contact with the sharp FBP edge (Fig. S18e and f†), demonstrating physical damage.

It was interesting to note that the FNPs aggregated and adhered to some of the *E. coli* cells, forming pits on the bacterial surface and leading to irregular shapes (Fig. S18g–i†). This implies that adhesion of FNPs onto the surface of *E. coli* may cause destruction of cell integrity, similar to other materials.<sup>13,33</sup> Although the FNPs may lead to disinfection *via* oxidation, the small spherical structure of FNPs with a low positive charge may result in weaker adhesion, piercing, or other physical action to bacteria cells compared with FBP.

## 4. Conclusions

In this study, magnetic FBP nanoflakes were synthesized, to be used for disinfection and removing bacteria from contaminated waters. The bacterial removal efficiency of FBP was systematically studied and compared with bare FNPs. Results showed that FBP could remove 97% of *E. coli* under the optimized experimental conditions (initial concentration of  $5 \times 10^8$  CFU mL<sup>-1</sup>, pH = 6, 25 °C, reaction time of 30 min, material dosage of 2 mg mL<sup>-1</sup>). FBP was still an effective disinfectant even in high salinity waters and in the presence of common anions at concentrations typical of most water sources. Moreover, 87% of *E. coli* cells could be removed by FBP even in the fifth reuse cycle, demonstrating good reusability. FBP performs better as a disinfectant than FNPs due to its composition and morphology: (1) the higher positive charge of FBP due to the addition of barium phosphate to FNPs improves electrostatic interactions, altering cell permeability and inducing plasmolysis; (2) the special two-dimensional flake structure of FBP with sharp edges and corners can induce the physical disruption of the bacterial cell membrane, releasing cellular components, and resulting in cell death, similar to magnetic graphene.<sup>34</sup> The removal and disinfection mechanisms of FBP include: electrostatic adhesion onto the surface, the flocculation effect of polyvalent cations, oxidation inactivation by Fe<sub>3</sub>O<sub>4</sub> in FBP, and irreversible cell damage by FBP's sharp structure. Cell damage from the sharp edges confirmed the low disinfection when FBP was added without mechanical mixing or stirring; shaking or stirring of FBP resulted in similarly high disinfection *via* cell damage. Generally, taking into account their easy preparation, magnetic separation, high removal efficiency, effective disinfection,

and good reusability, magnetic FBP nanoflakes are an ideal material for water disinfection.

## Conflicts of interest

There are no conflicts to declare.

## Acknowledgements

This work was financially supported by the Jiangsu Natural Science Foundation of China (Grant No. SBK2017020336), the Fundamental Research Funds for the Central Universities (Grant No. KYZ201747), and the National Natural Science Funds of China (Grant No. 51402153). This work was in part supported by the National Science Foundation (NSF) and the U.S. Environmental Protection Agency (EPA) under NSF-EF0830117. Any opinions, findings, conclusions or recommendations expressed in this material are those of the authors and do not necessarily reflect the views of the funding agencies.

## References

- 1 S. Zhan, Y. Yang, Z. Shen, J. Shan, Y. Li, S. Yang and D. Zhu, Efficient removal of pathogenic bacteria and viruses by multifunctional amine-modified magnetic nanoparticles, *J. Hazard. Mater.*, 2014, 274, 115–123.
- 2 S. Singh, K. Barick and D. Bahadur, Inactivation of bacterial pathogens under magnetic hyperthermia using Fe<sub>3</sub>O<sub>4</sub>–ZnO nanocomposite, *Powder Technol.*, 2015, 269, 513–519.
- 3 S. Zhan, D. Zhu, S. Ma, W. Yu, Y. Jia, Y. Li, H. Yu and Z. Shen, Highly efficient removal of pathogenic bacteria with magnetic graphene composite, *ACS Appl. Mater. Interfaces*, 2015, 7, 4290–4298.
- 4 Y. Jin, F. Liu, C. Shan, M. Tong and Y. Hou, Efficient bacterial capture with amino acid modified magnetic nanoparticles, *Water Res.*, 2014, 50, 124–134.
- 5 S. Herrmann, L. De Matteis, J. M. de la Fuente, S. G. Mitchell and C. Streb, Removal of Multiple Contaminants from Water by Polyoxometalate Supported Ionic Liquid Phases (POM-SILPs), *Angew. Chem., Int. Ed.*, 2017, 56, 1667–1670.
- 6 E. Roy, S. Patra, A. Tiwari, R. Madhuri and P. K. Sharma, Single cell imprinting on the surface of Ag–ZnO bimetallic nanoparticle modified graphene oxide sheets for targeted detection, removal and photothermal killing of *E. Coli*, *Biosens. Bioelectron.*, 2017, 89, 620–626.
- 7 L. Akhigbe, S. Ouki and D. Saroj, Disinfection and removal performance for *Escherichia coli* and heavy metals by silver-modified zeolite in a fixed bed column, *Chem. Eng. J.*, 2016, 295, 92–98.
- 8 M. Hassan, R. Abou-Zeid, E. Hassan, L. Berglund, Y. Aitomäki and K. Oksman, Membranes based on cellulose nanofibers and activated carbon for removal of *Escherichia coli* bacteria from water, *Polymer*, 2017, 9, 335.
- 9 T. Zou, C. Wang, R. Tan, W. Song and Y. Cheng, Preparation of pompon-like ZnO-PANI heterostructure and its applications for the treatment of typical water pollutants under visible light, *J. Hazard. Mater.*, 2017, 338, 276–286.

- 10 E. Anfruns-Estrada, C. Bruguera-Casamada, H. Salvadó, E. Brillas, I. Sirés and R. M. Araujo, Inactivation of microbiota from urban wastewater by single and sequential electrocoagulation and electro-Fenton treatments, *Water Res.*, 2017, **126**, 450–459.
- 11 S. Singh, K. Barick and D. Bahadur, Fe<sub>3</sub>O<sub>4</sub> embedded ZnO nanocomposites for the removal of toxic metal ions, organic dyes and bacterial pathogens, *J. Mater. Chem. A*, 2013, **1**, 3325–3333.
- 12 Y. Jiang, J.-L. Gong, G.-M. Zeng, X.-M. Ou, Y.-N. Chang, C.-H. Deng, J. Zhang, H.-Y. Liu and S.-Y. Huang, Magnetic chitosan-graphene oxide composite for anti-microbial and dye removal applications, *Int. J. Biol. Macromol.*, 2016, **82**, 702–710.
- 13 V. K. Sharma, T. J. McDonald, H. Kim and V. K. Garg, Magnetic graphene-carbon nanotube iron nanocomposites as adsorbents and antibacterial agents for water purification, *Adv. Colloid Interface Sci.*, 2015, **225**, 229–240.
- 14 K. Niemirowicz, I. Swiecicka, A. Z. Wilczewska, K. H. Markiewicz, U. Surel, A. Kułakowska, Z. Namiot, B. Szynaka, R. Bucki and H. Car, Growth arrest and rapid capture of select pathogens following magnetic nanoparticle treatment, *Colloids Surf., B*, 2015, **131**, 29–38.
- 15 S. Chella, P. Kollu, E. V. P. Komarala, S. Doshi, M. Saranya, S. Felix, R. Ramachandran, P. Saravanan, V. L. Koneru and V. Venugopal, Solvothermal synthesis of MnFe<sub>2</sub>O<sub>4</sub>-graphene composite—Investigation of its adsorption and antimicrobial properties, *Appl. Surf. Sci.*, 2015, **327**, 27–36.
- 16 J. Chen, B. Duncan, Z. Wang, L.-S. Wang, V. M. Rotello and S. R. Nugen, Bacteriophage-based nanoprobe for rapid bacteria separation, *Nanoscale*, 2015, **7**, 16230–16236.
- 17 F. Halouane, R. Jijie, D. Meziane, C. Li, S. K. Singh, J. Bouckaert, J. Jurazek, S. Kurungot, A. Barras and M. Li, Selective isolation and eradication of E. coli associated with urinary tract infections using anti-fimbrial modified magnetic reduced graphene oxide nanoheaters, *J. Mater. Chem. B*, 2017, **5**, 8133–8142.
- 18 S. Ma, S. Zhan, Y. Jia and Q. Zhou, Highly efficient antibacterial and Pb (II) removal effects of Ag-CoFe<sub>2</sub>O<sub>4</sub>-GO nanocomposite, *ACS Appl. Mater. Interfaces*, 2015, **7**, 10576–10586.
- 19 F. Zhang, X. Yin, J. Lan and W. Zhang, Application of Ba<sub>3</sub>(PO<sub>4</sub>)<sub>2</sub>/Fe<sub>3</sub>O<sub>4</sub> as a novel magnetic adsorbent to remove methyl blue from aqueous solution, *J. Mater. Sci.*, 2016, **51**, 3525–3535.
- 20 F. Zhang, X. Yin and W. Zhang, Development of magnetic Sr<sub>5</sub>(PO<sub>4</sub>)<sub>3</sub>(OH)/Fe<sub>3</sub>O<sub>4</sub> nanorod for adsorption of Congo red from solution, *J. Alloys Compd.*, 2016, **657**, 809–817.
- 21 F. Zhang, B. Ma, X. Jiang and Y. Ji, Dual function magnetic hydroxyapatite nanopowder for removal of malachite green and Congo red from aqueous solution, *Powder Technol.*, 2016, **302**, 207–214.
- 22 F. Zhang, Z. Wei, W. Zhang and H. Cui, Effective adsorption of malachite green using magnetic barium phosphate composite from aqueous solution, *Spectrochim. Acta, Part A*, 2017, **182**, 116–122.
- 23 F. Zhang, Z. Zhao, R. Tan, Y. Guo, L. Cao, L. Chen, J. Li, W. Xu, Y. Yang and W. Song, Selective and effective adsorption of methyl blue by barium phosphate nano-flake, *J. Colloid Interface Sci.*, 2012, **386**, 277–284.
- 24 X. Zhu, H. Fan, D. Li, Y. Xiao and X. Zhang, Protein adsorption and zeta potentials of a biphasic calcium phosphate ceramic under various conditions, *J. Biomed. Mater. Res., Part B*, 2007, **82**, 65–73.
- 25 Y. Jin, J. Deng, J. Liang, C. Shan and M. Tong, Efficient bacteria capture and inactivation by cetyltrimethylammonium bromide modified magnetic nanoparticles, *Colloids Surf., B*, 2015, **136**, 659–665.
- 26 L. C. Roberts, S. J. Hug, T. Ruettimann, M. M. Billah, A. W. Khan and M. T. Rahman, Arsenic removal with iron (II) and iron (III) in waters with high silicate and phosphate concentrations, *Environ. Sci. Technol.*, 2004, **38**, 307–315.
- 27 M. W. Tenney and W. Stumm, Chemical flocculation of microorganisms in biological waste treatment, *J. - Water Pollut. Control Fed.*, 1965, **37**, 1370–1388.
- 28 E. Neyens and J. Baeyens, A review of thermal sludge pre-treatment processes to improve dewaterability, *J. Hazard. Mater.*, 2003, **98**, 51–67.
- 29 W. Hu, C. Peng, W. Luo, X. Li, D. Li, Q. Huang and C. Fan, Graphene-Based Antibacterial Paper, *ACS Nano*, 2010, **4**, 4317–4323.
- 30 E. I. Rabea, M. E. T. Badawy, C. V. Stevens, G. Smagghe and W. Steurbaut, Chitosan as Antimicrobial Agent: Applications and Mode of Action, *Biomacromolecules*, 2003, **4**, 1457–1465.
- 31 N. Tran, A. Mir, D. Mallik, A. Sinha, S. Nayar and T. J. Webster, Bactericidal effect of iron oxide nanoparticles on Staphylococcus aureus, *Int. J. Nanomed.*, 2010, **5**, 277–283.
- 32 B. Stephen Inbaraj, T. Y. Tsai and B. H. Chen, Synthesis, characterization and antibacterial activity of superparamagnetic nanoparticles modified with glycol chitosan, *Sci. Technol. Adv. Mater.*, 2012, **13**, 015002.
- 33 S. Singh, K. Barick and D. Bahadur, Surface engineered magnetic nanoparticles for removal of toxic metal ions and bacterial pathogens, *J. Hazard. Mater.*, 2011, **192**, 1539–1547.
- 34 G. Gollavelli, C.-C. Chang and Y.-C. Ling, Facile synthesis of smart magnetic graphene for safe drinking water: heavy metal removal and disinfection control, *ACS Sustainable Chem. Eng.*, 2013, **1**, 462–472.